THE JOURNAL OF PHYSICAL CHEMISTRY Letters

pubs.acs.org/JPCL Letter

Interfacial Dynamics in Supported Ultrathin Polymer Films—From the Solid to the Free Interface

Emmanuel Urandu Mapesa, Nobahar Shahidi, Friedrich Kremer, Manolis Doxastakis,* and Joshua Sangoro*

Cite This: *J. Phys. Chem. Lett.* 2021, 12, 117−125 Read Online

ACCESS | Metrics & More | Article Recommendations | Supporting Information

ABSTRACT: Molecular dynamics in ultrathin layers is investigated using nanostructured electrodes to perform broadband dielectric spectroscopy measurements, and by atomistic molecular dynamics simulations. Using poly(vinyl acetate) as the model system and taking advantage of access to the distribution of relaxation times in an extended temperature range above the glass transition temperature, T_g, we demonstrate that while the mean rates of the segmental relaxation remain bulklike down to 12 nm film thickness, modified molecular mobilities arise in the interfacial zones. Combining results from simulations and experiments, we show unambiguously that both the slow relaxations arising from adsorbed polymer segments and the faster modes attributed to segments in the vicinity of the free interface have non-Arrhenius temperature activation. These interfacial regions span thicknesses of ∼1.5 nm each just above the calorimetric T_g independent of molecular weight and film thickness. These deviations at interfaces are relevant for applications of polymers in adhesion, coatings, and polymer nanocomposites.

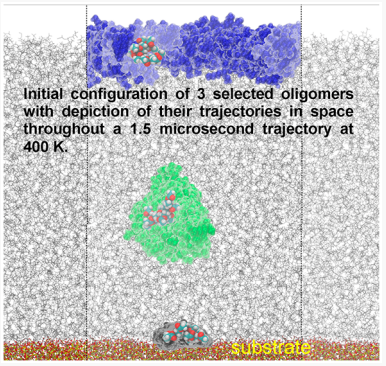

For close to three decades now, amorphous polymer thin films have received close scientific attention in pursuit of a fundamental understanding of the phenomena that occur in confinement, and because of the many possible practical applications, such as protective and lubricating coatings, smart window layers, adhesives, microelectronic encapsulants, and dielectrics.[1,2] Because interfacial interactions and free surfaces are expected to play a significant role in determining the overall properties of thin films as their thickness is reduced, recent focus has been directed toward designing experiments that give direct access to the interface, rather than those that probe the global characteristics of the films.[3−15] For example, Ellison and Torkelson inserted dye-labeled molecules in known positions of polystyrene films, and reported a distribution of T_gs through the expanse of the film from their fluorescence studies.[9] Using a similar approach, Paeng et al. estimate the thickness of a mobile surface layer in free and supported films to be ∼4 nm at T_g.[14] By probing dynamics in polymer blend films, Yin et al. conclude that the T_g shifts arise due to a mobile layer that preferentially assembles at the surface.[13] Theoretical and computational approaches have made a case for the existence of different dynamic regimes in thin films, and especially limited mobility in the first adsorbed layer.[16−26] The existence of a gradient of mobilities and glass transition temperatures in different regions of the confined material has been demonstrated and dependence on the nature of the supporting substrate explored.[22,25] Slower and more heterogeneous chain and segmental dynamics near the substrate have been reported for different polymer films interacting with unattractive surfaces[21,27,28] with an additional relaxation mode that is not present in bulk.[19,23,24] A common string running through the aforementioned experimental efforts is the fact that they make use of an indirect approach to probing the dynamics of interest. In using dye-labeled molecules, for instance, it is implicitly assumed that there is complete coupling of probe dynamics to the host polymer's relaxation, and that the dye labels are uniformly distributed throughout the film.

In the present work—distinct from previous efforts[29,30] that involved evaporation of metal electrodes onto polymer layers hence introducing potential artifactual effects on the measured dynamics[31]—a *nondestructive* approach that employs BDS in combination with a nanostructured electrode arrangement[8,32−34] is used to probe the dynamics of neat poly(vinyl acetate) (PVAc) in the vicinity of solid and free interfaces. It is demonstrated that although the mean relaxation times for thin PVAc films remain bulklike, there are additional relaxation modes that arise due to confinement. We perform atomistic molecular dynamics (MD) simulations utilizing a sample geometry that closely mimics experimental conditions and show evidence of modified mobility at the interfaces: an additional slow process, with Vogel−Fulcher−Tammann (VFT)-like temperature activation, emerges due to adsorption

Received: October 26, 2020
Accepted: November 30, 2020
Published: December 14, 2020

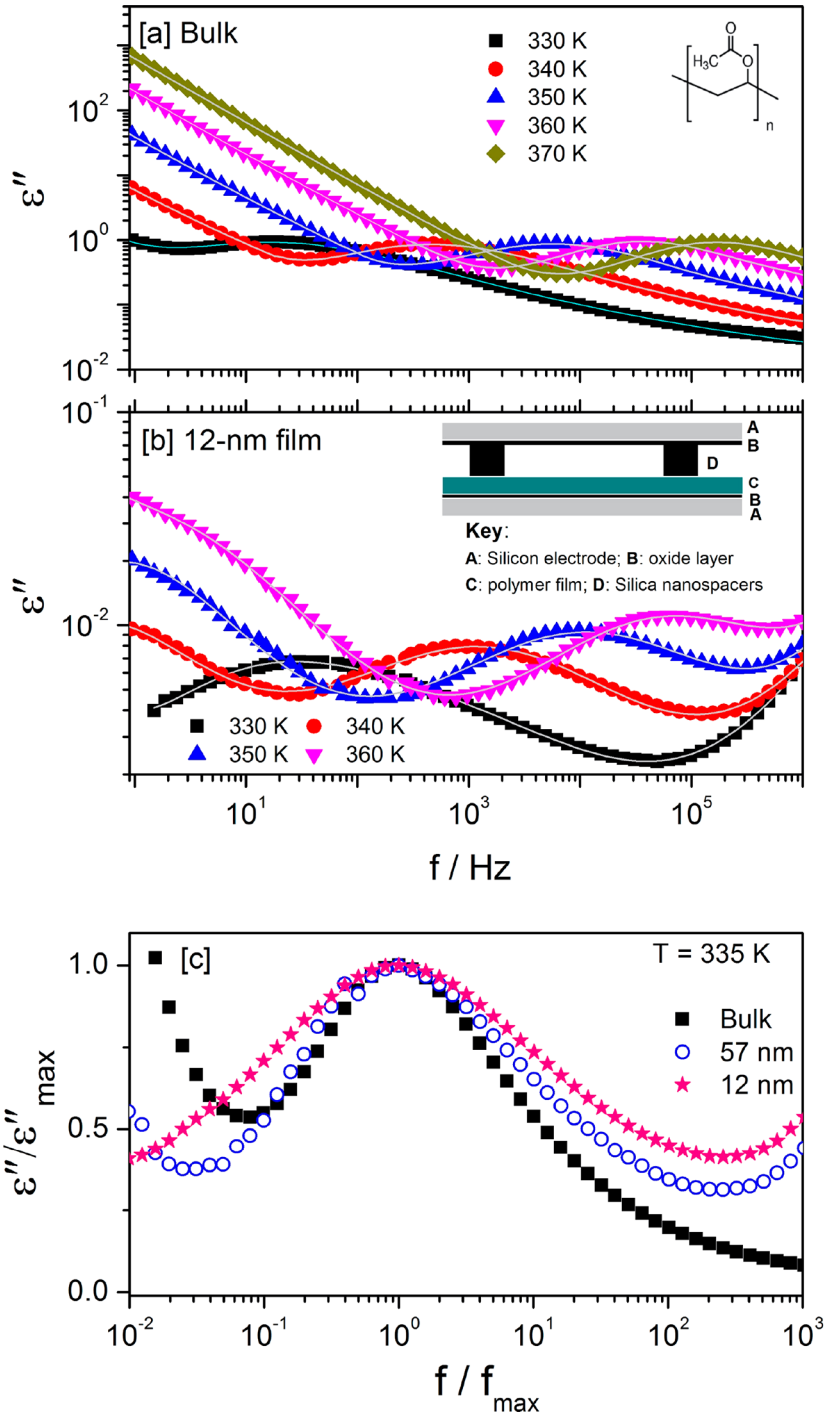

Figure 1. Imaginary part of the complex dielectric function, $\varepsilon^* = \varepsilon' - i\varepsilon''$, as measured for (a) a bulk sample and (b) a supported 12 nm thin layer of poly(vinyl acetate) (PVAc), M_w = 110 kg/mol. For graphical clarity, data is displayed only for a select set of temperatures. The solid lines are fits as described in the text (see the SI for details on fitting thin film data). (c) Dielectric loss as a function of frequency, for samples with different thicknesses as indicated, normalized with respect to the maximum loss value of the segmental relaxation as well as the respective frequency position. Insets: (a) chemical structure of PVAc; (b) schematic representation of the sample geometry used for BDS measurements of thin polymer samples. The error bars are comparable to the size of the symbols unless otherwise indicated.

of the polymer on the silica surface, while polymer segments in the immediate vicinity of the free interface have accelerated mobility and also bear non-Arrhenius temperature activation.

Figure 1 shows raw dielectric data as measured at different temperatures for a bulk sample (Figure 1a) of PVAc (M_w = 110 kg/mol, PID = 2) and a 12 nm thin film of the same sample (Figure 1b). The bulk data is dominated by two processes that show up as a peak and a flank on the low-frequency side representing segmental relaxation and dc ionic conductivity, respectively. These spectra can be adequately described (see the solid lines in Figure 1a) by a combination of the empirical Havriliak–Negami (HN) function[35] and a term accounting for the conductivity contribution: $\varepsilon^*(\omega) = -i\frac{\sigma_0}{\omega\varepsilon_0} + \varepsilon_\infty + \frac{\Delta\varepsilon}{(1+\{i\omega\tau_{HN}\}^\beta)^\gamma}$, where $\varepsilon^* = \varepsilon' - i\varepsilon''$ is

https://dx.doi.org/10.1021/acs.jpclett.0c03211
J. Phys. Chem. Lett. 2021, 12, 117−125

the complex dielectric function; σ_0, ε_0, ε_∞, $\Delta\varepsilon$, τ_{HN}, β, and γ are the dc conductivity of the sample, the dielectric permittivity of vacuum, the permittivity of the unrelaxed medium, the dielectric relaxation strength, the characteristic relaxation time of the HN model, and the symmetric and asymmetric shape parameters, respectively; and $\omega = 2\pi f$ is the angular frequency of the applied external field.

Figure 1c shows dielectric loss data measured at 335 K for PVAc (M_w = 110 kg/mol) bulk and two thin film samples. A similar plot for the other molecular weight (157 kg/mol) studied is provided in Figure S1. The data—normalized with respect to the maximum loss value of the segmental relaxation—reveals no shift in the mean frequency position of the loss maximum. Clearly, the spectra for the thin films have more features arising from several contributions (see the schematic in the inset, Figure 1b), namely, the thermally oxidized silica layer on the Si wafers, the silica nanospacers, the polymeric film, the (air) gap between the film layer and the spacers, and the wafers. All these contributions are considered when fitting the measured functions; the details are published elsewhere[36] and briefly explained in the Supporting Information. To describe the contribution of the polymer layer, we use three HN functions (Figure 2a) to account for the structural relaxation, and two additional processes that show up—one as a hump on the low-frequency side, and the other on the high-frequency side. We refer to them in the rest of this work as α_{slow} and α_{fast}, respectively, and are able to follow them albeit within a narrow temperature range. As will be shown later, we have carried out atomistic simulations which provide further evidence for the presence of these additional modes.

From Figure 2, we make several pertinent observations: First, a process, α_{slow}, slower than the structural relaxation by ~2 decades (at high temperatures) shows up for the thin films. The shape of this relaxation does not seem to change with temperature (not shown) but clearly broadens symmetrically with film thickness (Figure 2a). We ascribe this slow process to adsorbed polymer segments or those close to them at the substrate/polymer interface; their motion is hindered by the physical constraints, hence conformational changes, imposed on them. Recently, Cheng and Sokolov reported a similar process in PVAc nanocomposites and alluded it to an interfacial layer in the immediate vicinity of the nanoparticles.[37] It is important to note here that while these effects are observed in nanocomposites, thin polymer films allow for investigation in a precisely controlled flat geometric confinement.[38−40] Second, α_{fast}, a process faster than the structural relaxation, is present, and its shape shows dependence on both film thickness and temperature. This process is assigned to polymer segments at the polymer/air interface which have more degrees of freedom in their response to an external perturbation. It narrows down almost symmetrically with film thickness, suggesting that the further away the *free segments* are from the polymer/solid interface, the less heterogeneous their relaxation becomes. As temperature is increased, their relaxation becomes more homogeneous, hence the narrowing of the peak. Third, we observe that, compared to bulk, the α-relaxation is barely changed in its spectral position and shape down to the thinnest film (12 nm) studied. The fact that the mean structural relaxation times in the thin films are identical to those in the bulk system implies that the dynamic glass transition is, in this respect, not influenced by confinement. Using local dielectric spectroscopy—which also offers one free interface—Nguyen et al. have studied PVAc thin films on

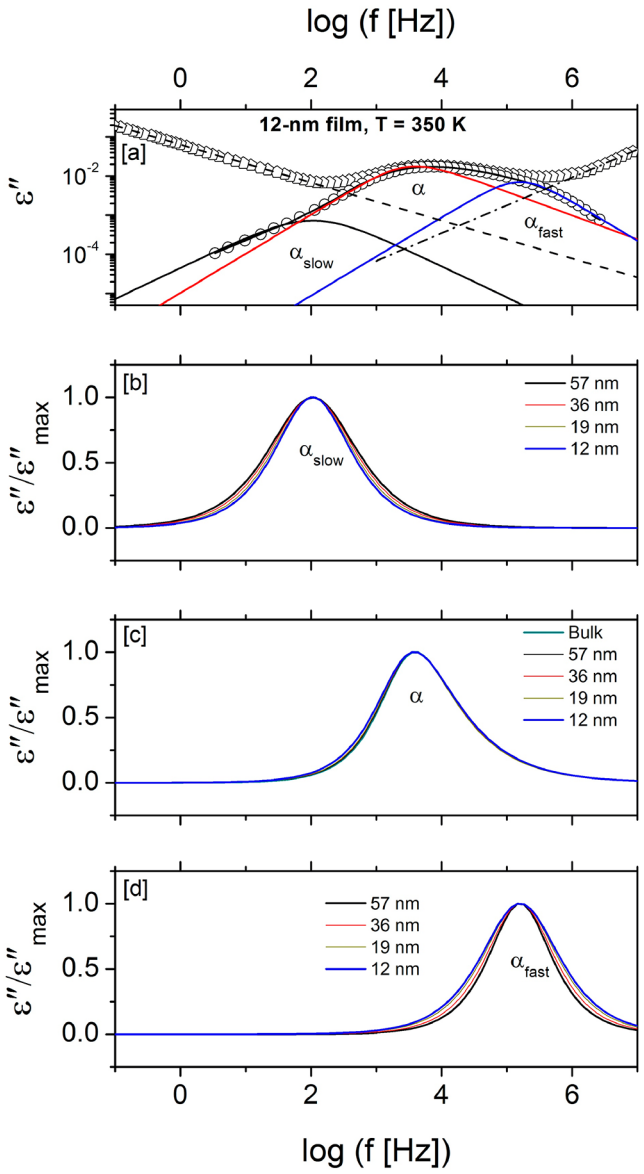

Figure 2. (a) Demonstration of the fitting of the dielectric loss data measured at 350 K for a 12 nm thin film of PVAc (M_w = 110 kg/mol). First, the low- and high-frequency flanks (dash and dash−dotted lines, respectively) are subtracted from the as-measured data (open pentagons) thereby resulting in a corrected spectrum (open circles). To describe the corrected spectrum, three Havriliak−Negami functions are needed, thereby helping identify three relaxation processes α_{slow}, α, and α_{fast} as indicated. (b−d) HN functions for the three processes displayed for different samples with varying thicknesses. The error bars are comparable to the size of the symbols unless otherwise indicated.

various substrates and find that the segmental dynamics of a 12 nm thin film supported on silicon has bulklike dynamics in terms of both the mean relaxation rates and the width of the relaxation peak.[41] Put together, these observations help build a concise picture of the effect of geometrical confinement on macromolecules. This picture can explain the reason for disparity in the results reported for dynamics in thin films over the past several decades. It is likely that reports of drastic suppression or enhancement of the glass transition temperature in thin films, especially by ellipsometric studies, are a result of a procedure that gives greater weighting to either the

https://dx.doi.org/10.1021/acs.jpclett.0c03211
J. Phys. Chem. Lett. 2021, 12, 117−125

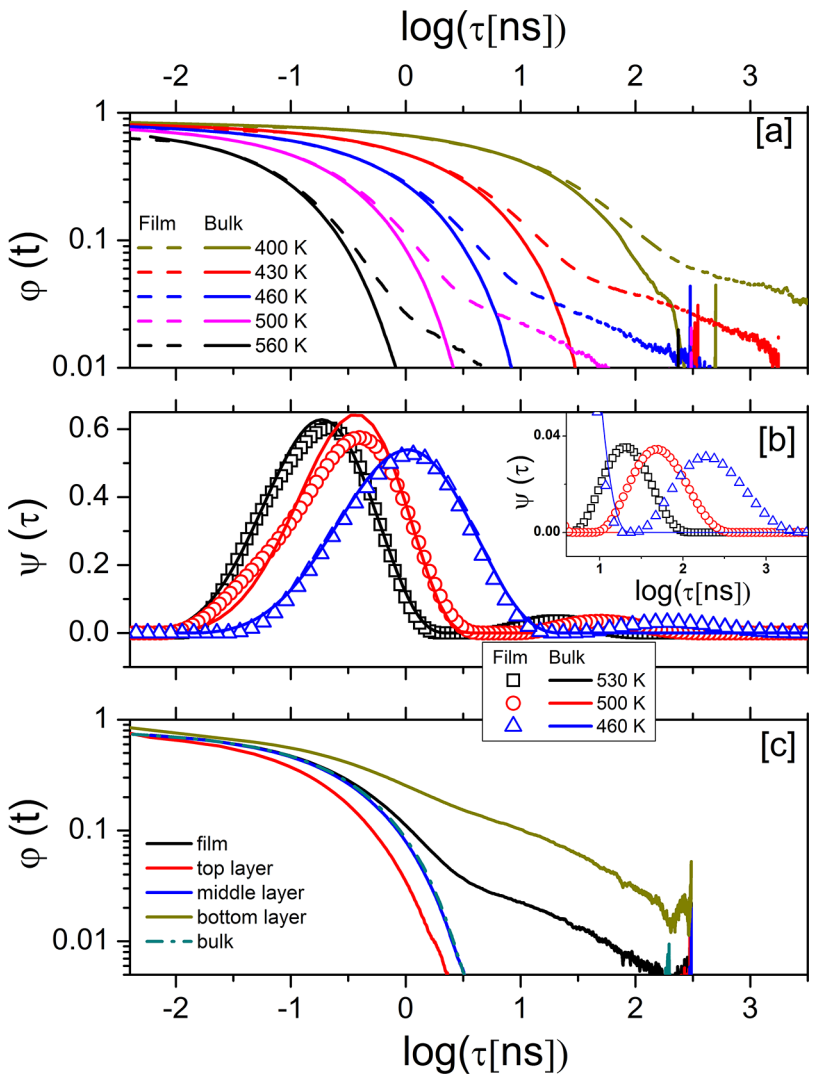

Figure 3. (a) Monomer dipole autocorrelation function (φ) for film (symbols) and bulk (dashed lines) at five temperatures: 400, 430, 460, 500, and 560 K. (b) Distribution of relaxation times for thin film (symbols) and bulk (dashed lines) at 460, 500, and 530 K. The inset in part b is a zoom-in into the long-time side of the graph. (c) Monomer dipole autocorrelation function for different layers and the total film compared to bulk at the same temperature (500 K).

"free segments" at the top of the film or the "constrained segments" at the solid interface, respectively. This fact has been alluded to by the work of Forrest and Dalnoki-Veress who advance a model which shows that what is typically measured as a dilatometric glass transition temperature—characterized by a kink in the temperature dependence of film thickness or index of refraction—only represents the dynamics of a small fraction of the sample.[42] On the other hand, techniques like BDS and ac chip calorimetry which probe the whole sample volume report an average of all relaxation times available; if therefore focus is paid only to the mean relaxation times of the molecular process of interest, and not their distribution, some effects of confinement may go unnoticed.[43]

MD simulations were performed with a model that encompasses full atomistic detail and partial charges to examine the range of segmental dynamics throughout the film using the same metric probed in experiments: the segment dipole autocorrelation function. Recent computational studies with weakly interacting apolar models emphasized that, beyond density effects, torsional barriers present in atomistic models of polymers contribute to sorption/desorption dynamics at low temperatures and proposed an Arrhenius dependence for residence times on surfaces.[19,23,24] These studies also suggested that dielectric relaxation should remain unimodal albeit with a broader dielectric loss, but no comparison to experimental data was offered. Within this study, the strong interactions of PVAc with the silica allow for a direct probe of distinct surface dynamics through microsecond-long simulations at elevated temperatures offering together with BDS an unprecedented broad view of dipolar relaxation on surfaces over a range spanning at least 200 K.

Segmental dynamics are quantified in the time domain by calculating the monomer dipole autocorrelation function in the z-component (φ) from the MD trajectory as $\varphi(\Delta t) = \langle \vec{\mu}_z(t + \Delta t)\cdot\vec{\mu}_z(t)\rangle / \langle \vec{\mu}_z(t)\cdot\vec{\mu}_z(t)\rangle$, where $\vec{\mu}_z(t) = \sum_i q_i \cdot \vec{r}_i \cdot \hat{e_z}(t)$ is the z-component of the monomer dipole moment at time t, and q and r represent the partial charge and position of the atoms, respectively. Dynamics are probed in the z direction for comparison with BDS data.[44] Relaxation of the monomer dipole autocorrelation of bulk PVAc follows other measures of segmental relaxation such as

https://dx.doi.org/10.1021/acs.jpclett.0c03211
J. Phys. Chem. Lett. 2021, 12, 117−125

torsional autocorrelation functions (as shown in Figure S2), a feature that has been observed for other molecules as well.[45] Segmental dynamics in film and bulk PVAc at different temperatures are compared in Figure 3a. The initial steep drop in the autocorrelation function is due to fast-vibrational motion. This librational relaxation occurs at time steps smaller than times depicted in the figure for both film and bulk. At short times, the trend in films is identical to bulk, but it diverges at longer time scales where an additional relaxation mode becomes prominent. This second relaxation is related to decelerated polymer segments on the silica substrate,[20,21,23,24] hence corroborating our experimental dielectric results.

In order to obtain a comprehensive picture of the different relaxations and compare the simulation results with BDS data, the distribution of Debye relaxation times was extracted[46−48] as $\varphi_C(t) = \sum_\tau \psi(\log(\tau))e^{(-t)/(\tau)}$, where φ_C is fitted to φ, and $\psi(\log(\tau))$ is the weight of segments with characteristic relaxation time τ. Figure 3b shows the distribution of Debye relaxation times for thin films and bulk at different temperatures. The slow process is not well-described by the fits because of its small contribution to the overall autocorrelation function and the high error in the data at longer times. Consequently, the distribution of relaxation times shows a sharp peak for the slow process which does not match φ exactly and, as shown by the Kohlrausch−Williams−Watts (KWW) fits,[49] should be more heterogeneous. Nevertheless, the fits show the overall trends of relaxation times in film compared to bulk. As observed in the dielectric loss graphs from BDS experiments (Figure 1c) and simulations (Figure 3), the range of relaxation times is broader in films, with both smaller and larger times than bulk (see also Figure S3 where experimental data is directly compared to simulations). There are two separate modes present in the thin films as revealed by simulations, indicating two different relaxation processes. As previously mentioned, the peak at longer relaxation times arises from adsorbed segments at the polymer/substrate interface due to strong interactions mediated by the presence of hydrogen bonds between the polymer and silanol groups. The relaxation mode occurring at short times in the films coincides with the primary relaxation in the bulk system and is therefore unambiguously assigned to the dynamic glass transition.

For the films, an additional distribution is observed at short relaxation times due to the presence of the free interface which, unlike the attractive substrate, does not present a strong deviation in segmental dynamics. The relative strength of the slow process in thin films is small compared to the main peak, but it increases with reducing temperature. This explains why the contribution by the slow process to the overall spectra is stronger in the experimental data than in the simulated data (note that simulations are carried out at relatively higher temperature than experiments). Now, by defining regions in the film (i.e., bottom, middle, and top layer) and probing their respective segmental dynamics by MD simulations (see Figures S4−S6), we find that the effect of the interfaces is short ranged given the fact that the middle layer has identical dynamics to bulk (Figure 3c). Evidently, the dynamics of the film are dominated by the middle layer which has the highest mole fraction. The additional slow relaxation mode is only present in the adsorbed layer. Both the bottom layer that exhibits the second mode and the top layer have a range of 3−4 nm throughout the temperature range (430−560 K). The portion of segments at these layers does not show a strong temperature dependence. There are two relaxation processes at the bottom layer: the main relaxation which is similar to bulk, and a second relaxation mode with longer τ, responsible for the slow and heterogeneous dynamics close to the substrate. The mean relaxation time is smaller at the top layer, but its distribution has strong overlap with the middle layer. The fast motion of segments close to the free surface has a small contribution to overall film dynamics. Evidently, therefore, the picture to be drawn from these findings is that of segmental mobilities that are, on average, faster than bulk at the free interface but steadily slow down to reach bulklike rates in the middle of the polymer before gradually slowing down further as a "*gedanken*" probe approaches the solid interface.

In Figure 4, we present the temperature dependence of the characteristic mean relaxation times of the main segmental

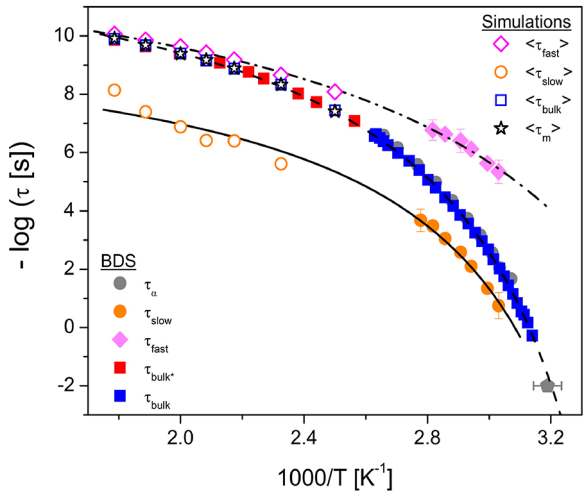

Figure 4. Relaxation map for different processes in films (circles) and bulk (squares) from simulations (open symbols) and BDS experiments (filled symbols). High-temperature BDS data, τ_{bulk*}, is taken from the literature.[50] The solid, dash, and dash−dotted lines represent VFT fits to the slow, segmental, and fast processes, respectively, with parameters log τ_0 = (9.1, 12.1, 11.9); DT_V = (1093.5, 1409.2, 1472.5 K), and T_V = (271.9, 268.8, 232.3 K). The pentagon symbol represents T_g for the bulk system determined by differential scanning calorimetry. The error bars are comparable to the size of the symbols unless otherwise indicated.

process (τ_m, from experiments and simulations for both bulk and thin films), and that of τ_{slow} and τ_{fast} present in the films. For simulation, τ_m and τ_{slow} are mean relaxation times from KWW fits[49] of the film, and τ_{fast} is extracted by fitting the top layer (as explained in the SI), while for experimental data, they are calculated from HN parameters as $\tau = \tau_{HN} \sin(\beta\gamma\pi)/([2 + 2\gamma])^{1/\beta} \sin(\beta\pi/[2 + 2\gamma])^{-1/\beta}$. Instructively, errors in simulation results are caused by a several factors: the limited statistics at low temperatures due to long relaxation times beyond the capacity of state-of-the-art software; a low finite probability for whole molecules to adsorb on the substrate contributing to an average relaxation that potentially is slower due to the short chains modeled; and the fact that decomposition to separate processes involves numerical errors. Nonetheless, evidently, values of τ_m extracted from experimental and simulation data for thin films and bulk PVAc coincide, and their temperature dependence can be described by a single Vogel−Fulcher−Tammann (VFT) function,[51−53] $1/\tau_m(T) = (1/\tau_0) \exp(-DT_V)/[T - T_V])$, where τ_0 and D are constants, and T_V is the Vogel temperature. VFT-like dependence of the

https://dx.doi.org/10.1021/acs.jpclett.0c03211
J. Phys. Chem. Lett. 2021, 12, 117−125

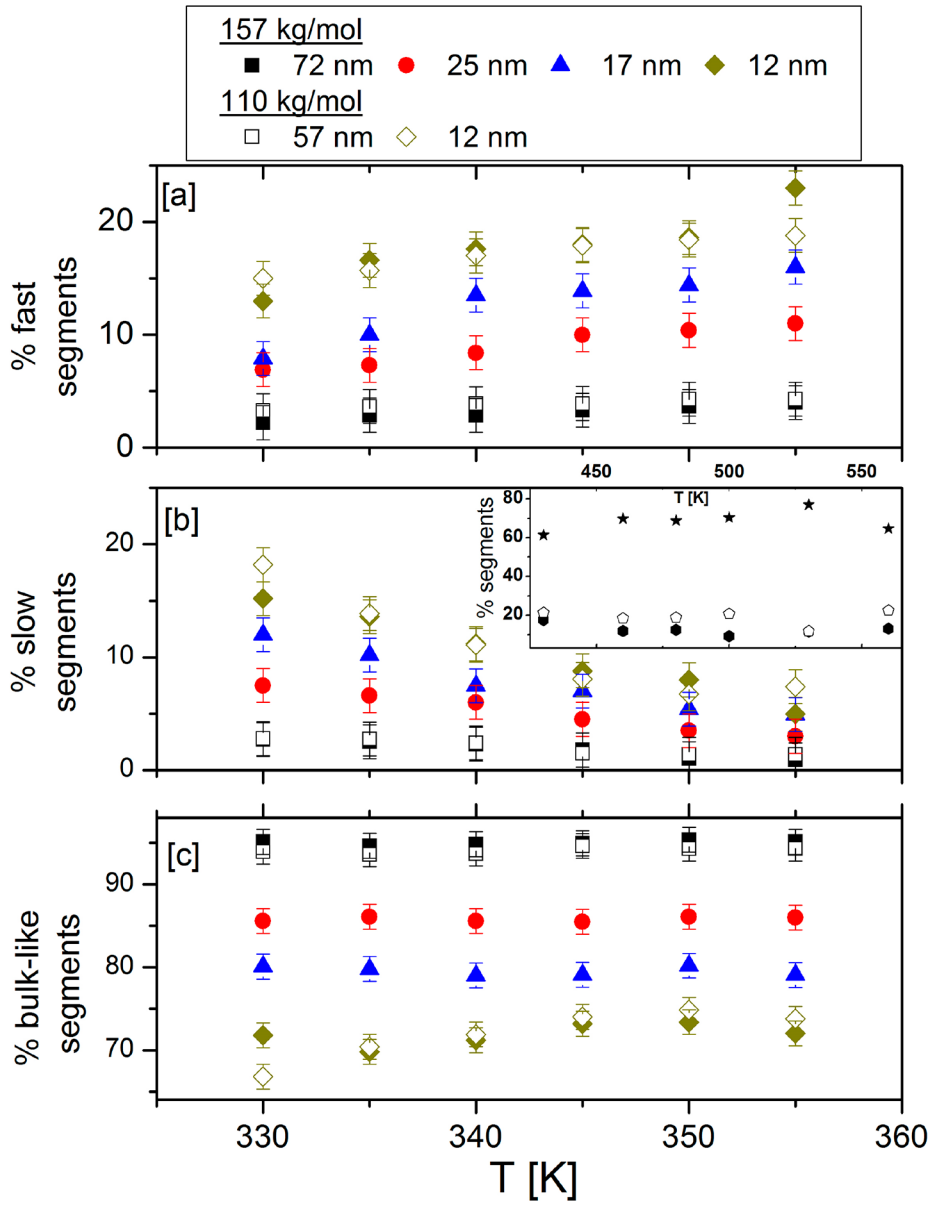

Figure 5. Percentage of segments whose mobility, relative to the bulk system, is (a) fast, (b) slowed down, and (c) bulklike, expressed as functions of temperature for films prepared from two different molecular weights of PVAc, as indicated. The inset in part b shows the temperature dependence of the fraction of segments with fast (filled hexagons), slowed down (empty pentagons), and bulklike (stars) mobility as determined from simulations.

structural relaxation times is characteristic of glassy systems and conventionally delivers a dynamically determined glass transition temperature, T_g, value for the system when extrapolated to a relaxation time of 100 s, as evident in Figure 4. There is disparity in the literature concerning whether the slow process arising from the solid/polymer interface has Arrhenius or non-Arrhenius temperature dependence.[54−56] By combining experimental and simulation results, we unambiguously show that both τ_{slow} and τ_{fast} have VFT-like activation for systems studied herein (see the caption of Figure 4 for fit parameters).

Having so far established a picture of varying molecular mobilities through the expanse of a supported thin polymer film, one must answer the following question: what fraction of segments have modified mobility compared to bulk? Given the fact that three HN functions are required to fit the dielectric loss data, we use their respective dielectric strengths $\Delta\varepsilon_i$ to estimate these fractions as $f_a = \Delta\varepsilon_a/(\Delta\varepsilon_a + \Delta\varepsilon_b + \Delta\varepsilon_c)$ (see Figures S7 and S8). Figure 5 shows the results of this analysis. Here, in the low-temperature regime probed by dielectric spectroscopy, the following is evident: (i) The fraction of segments with increased mobility grows, and that with slowed mobility diminishes with temperature. (ii) The magnitude of the portions of segments with altered mobility has no obvious dependence on molecular weight. (iii) Independent of film thickness and molecular weight, the fraction of segments that retain bulklike mobility is unchanged with temperature. As the inset in Figure 5 shows, the values of all the three portions of segments remain constant with temperature as revealed from simulations. We opine that this is the case at the high temperatures accessed by simulations; indeed, a plateauing out of the values is evident from the experimental data. Taking cue from the density profile in the film (Figure S9), the segments with faster mobility are assigned to be at the free interface;

https://dx.doi.org/10.1021/acs.jpclett.0c03211
J. Phys. Chem. Lett. 2021, 12, 117−125

those with reduced mobility are in the vicinity of the solid interface, while those with bulklike ones lie in the middle. As a first estimate of the length scales of these three regions, we assume constant segmental density throughout the film and calculate the corresponding sizes as fractions of the overall film thickness (known from atomic force microscopy measurements). The results of this estimate (Figure S10) reveal, close to the glass transition temperature, a length scale of about 1.5 nm, independent of film thickness and molecular weight, for both regions with modified mobility. While recent studies[14,57−59] have provided a characterization of the faster-than-bulk layer in thin films, to the best of our knowledge, no previous work has substantively probed the temperature, molecular-weight, and film-thickness dependence of the sizes of the regions with modified mobilities as done in this work.

In summary, BDS and MD simulations have been combined to probe dynamics in ultrathin PVAc polymer films in comparison to their bulk counterpart. Evidence is presented to show that while the mean structural relaxation times—and hence the glass transition temperature—in the thin films remain bulklike, altered dynamics arise in the vicinity of the interfaces. New molecular processes, one faster than and the other slower than structural relaxation of the bulk system, are observed and, by combining BDS and computational results, found to have VFT-like temperature dependence. The layer at the polymer/air interface bears dynamics faster than the bulk system, but their distribution strongly overlaps with that of the bulk. Instructively, the main segmental relaxation that is dominant away from the two interfaces has a similar distribution of relaxation times as well as temperature dependence to the bulk.

■ ASSOCIATED CONTENT

Supporting Information

The Supporting Information is available free of charge at https://pubs.acs.org/doi/10.1021/acs.jpclett.0c03211.

Experimental details, dielectric data and analysis, and MD simulations details (PDF)

■ AUTHOR INFORMATION

Corresponding Authors

Manolis Doxastakis − *Department of Chemical and Biomolecular Engineering, University of Tennessee Knoxville, Knoxville, Tennessee 37996, United States;* orcid.org/0000-0002-9175-9906; Email: edoxasta@utk.edu

Joshua Sangoro − *Department of Chemical and Biomolecular Engineering, University of Tennessee Knoxville, Knoxville, Tennessee 37996, United States;* orcid.org/0000-0002-5483-9528; Email: jsangoro@utk.edu

Authors

Emmanuel Urandu Mapesa − *Department of Chemical and Biomolecular Engineering, University of Tennessee Knoxville, Knoxville, Tennessee 37996, United States;* orcid.org/0000-0002-2206-0990

Nobahar Shahidi − *Department of Chemical and Biomolecular Engineering, University of Tennessee Knoxville, Knoxville, Tennessee 37996, United States*

Friedrich Kremer − *Department of Molecular Physics, Peter Debye Institute of Soft Matter Physics, University of Leipzig, 04103 Leipzig, Germany*

Complete contact information is available at: https://pubs.acs.org/10.1021/acs.jpclett.0c03211

Author Contributions

E.U.M., J.S., and F.K. conceived the experiments. M.D. initiated the simulations, and J.S. guided the project. E.U.M. and J.S. analyzed the experimental data, while N.S. and M.D. analyzed the simulations results. E.U.M. and N.S. cowrote the manuscript; all coauthors read and revised the manuscript.

Notes

The authors declare no competing financial interest.

■ ACKNOWLEDGMENTS

E.U.M. and J.S. are grateful for support from the National Science Foundation, Division of Materials Research, Polymers Program, award DMR-1905597. N.S. acknowledges funding from the Chancellor's Fellowship, UTK. F.K. appreciates financial support from the German Research Foundation via the Transregional Center for Collaborative Research SFB TRR 102 within the project, "Polymers under multiple constraints: restricted and controlled molecular order and mobility."

■ DEDICATION

This Letter is dedicated to Prof. Yuri Feldman on the occasion of his 70th birthday.

■ REFERENCES

(1) Kumar, S. K.; Vacatello, M.; Yoon, D. Y. Off-lattice Monte Carlo simulations of polymer melts confined between two plates. *J. Chem. Phys.* **1988**, *89*, 5206−5215.

(2) Petychakis, L.; Floudas, G.; Fleischer, G. Chain dynamics of polyisoprene confined in porous media. A dielectric study. *Europhys. Lett.* **1997**, *40*, 685−690.

(3) Fakhraai, Z.; Forrest, J. A. Measuring the surface dynamics of glassy polymers. *Science* **2008**, *319*, 600−604.

(4) Jones, R. A. L. Glasses with liquid-like surfaces. *Nat. Mater.* **2003**, *21*, 645−646.

(5) Cheng, S.; Carroll, B.; Bocharova, V.; Carrillo, J. M.; Sumpter, B. G.; Sokolov, A. P. Focus: Structure and dynamics of the interfacial layer in polymer nanocomposites with attractive interactions. *J. Chem. Phys.* **2017**, *146* (20), 203201.

(6) Lin, Y.; Liu, L.; Xu, G.; Zhang, D.; Guan, A.; Wu, G. Interfacial interactions and segmental dynamics of poly(vinyl acetate)/silica nanocomposites. *J. Phys. Chem. C* **2015**, *119*, 12956−12966.

(7) Madkour, S.; Yin, H.; Fullbrandt, M.; Schönhals, A. Calorimetric evidence for a mobile surface layer in ultrathin polymeric films: poly(2-vinyl pyridine). *Soft Matter* **2015**, *11*, 7942−52.

(8) Tress, M.; Mapesa, E. U.; Kossack, W.; Kipnusu, W. K.; Reiche, M.; Kremer, F. Glassy dynamics in condensed isolated polymer chains. *Science* **2013**, *341*, 1371−1374.

(9) Ellison, C. J.; Torkelson, J. M. The distribution of glass-transition temperatures in nanoscopically confined glass formers. *Nat. Mater.* **2003**, *2*, 695−700.

(10) Napolitano, S.; Wübbenhorst, M. The lifetime of the deviations from bulk behaviour in polymers confined at the nanoscale. *Nat. Commun.* **2011**, *2*, 260−266.

(11) Napolitano, S.; Cangialosi, D. Interfacial Free Volume and Vitrification: Reduction in Tg in proximity of an adsorbing interface explained by the free volume holes diffusion model. *Macromolecules* **2013**, *46*, 8051−8053.

(12) Chowdhury, M.; Priestley, R. D. Discrete mobility on the surface of glasses. *Proc. Natl. Acad. Sci. U. S. A.* **2017**, *114*, 4854−4856.

(13) Yin, H.; Madkour, S.; Schönhals, A. Unambiguous evidence for a highly mobile surface layer in ultrathin polymer films by specific heat spectroscopy on blends. *Macromolecules* **2015**, *48*, 4936−4941.

(14) Paeng, K.; Richert, R.; Ediger, M. D. Molecular mobility in supported thin films of polystyrene, poly(methyl methacrylate), and poly(2-vinyl pyridine) probed by dye reorientation. *Soft Matter* **2012**, *8*, 819−826.
(15) Mapesa, E. U.; Street, D. P.; Heres, M. F.; Kilbey, S. M.; Sangoro, J. Wetting and chain packing across interfacial zones affect distribution of relaxations in polymer and polymer-grafted nanocomposites. *Macromolecules* **2020**, *53*, 5315−5325.
(16) Baljon, A. R.; Billen, J.; Khare, R. Percolation of immobile domains in supercooled thin polymeric films. *Phys. Rev. Lett.* **2004**, *93*, 255701.
(17) Jain, T. S.; de Pablo, J. J. Investigation of transition States in bulk and freestanding film polymer glasses. *Phys. Rev. Lett.* **2004**, *92*, 155505.
(18) Lund, R.; Willner, L.; Alegria, A.; Colmenero, J.; Richter, D. Self-concentration and interfacial fluctuation effects on the local segmental dynamics of nanostructured diblock copolymer melts. *Macromolecules* **2008**, *41*, 511−514.
(19) Barrat, J.-L.; Baschnagel, J.; Lyulin, A. Molecular dynamics simulations of glassy polymers. *Soft Matter* **2010**, *6*, 3430−3446.
(20) Yelash, L.; Virnau, P.; Binder, K.; Paul, W. Three-step decay of time correlations at polymer-solid interfaces. *Europhys. Lett.* **2012**, *98*, 28006.
(21) Rissanou, A. N.; Harmandaris, V. Dynamics of various polymer-graphene interfacial systems through atomistic molecular dynamics simulations. *Soft Matter* **2014**, *10*, 2876−88.
(22) Mortazavian, H.; Fennell, C. J.; Blum, F. D. Structure of the interfacial region in adsorbed poly(vinyl acetate) on silica. *Macromolecules* **2016**, *49*, 298−307.
(23) Yelash, L.; Virnau, P.; Binder, K.; Paul, W. Slow process in confined polymer melts: layer exchange dynamics at a polymer solid interface. *Phys. Rev. E Stat. Nonlin. Soft Matter Phys.* **2010**, *82*, 050801.
(24) Mathieu, S.; Binder, K.; Paul, W. Dielectric relaxation of a polybutadiene melt at a crystalline graphite surface: atomistic molecular dynamics simulations. In *Dynamics in Geometrical Confinement*; Kremer, F., Ed.; Springer International Publishing: Berlin, 2014; pp 1−15.
(25) Phan, A. D.; Schweizer, K. S. Theory of spatial gradients of relaxation, vitrification temperature and fragility of glass-forming polymer liquids near solid substrates. *ACS Macro Lett.* **2020**, *9*, 448−453.
(26) White, R. P.; Lipson, J. E. G. To understand film dynamics look to the bulk. *Phys. Rev. Lett.* **2020**, *125*, 058002.
(27) Pandey, Y. N.; Brayton, A.; Burkhart, C.; Papakonstantopoulos, G. J.; Doxastakis, M. Multiscale modeling of polyisoprene on graphite. *J. Chem. Phys.* **2014**, *140*, 054908.
(28) Guseva, D. V.; Komarov, P. V.; Lyulin, A. V. Molecular-dynamics simulations of thin polyisoprene films confined between amorphous silica substrates. *J. Chem. Phys.* **2014**, *140*, 114903.
(29) Serghei, A.; Tress, M.; Kremer, F. Confinement effects on the relaxation time distribution of the dynamic glass transition in ultrathin polymer films. *Macromolecules* **2006**, *39*, 9385−9387.
(30) Fukao, K.; Uno, S.; Miyamoto, Y.; Hoshino, A.; Miyaji, H. Dynamics of alpha and beta processes in thin polymer films: poly(vinyl acetate) and poly(methyl methacrylate). *Phys. Rev. E: Stat. Phys., Plasmas, Fluids, Relat. Interdiscip. Top.* **2001**, *64*, 051807.
(31) Mapesa, E. U.; Erber, M.; Tress, M.; Eichhorn, K. J.; Serghei, A.; Voit, B.; Kremer, F. Glassy dynamics in nanometer thin layers of polystyrene. *Eur. Phys. J.: Spec. Top.* **2010**, *189*, 173−180.
(32) Serghei, A.; Kremer, F. Broadband dielectric studies on the interfacial dynamics enabled by use of nanostructured electrodes. *Rev. Sci. Instrum.* **2008**, *79*, 026101.
(33) Serghei, A.; Kremer, F. Broadband dielectric spectroscopy on ultrathin organic layers having one free (upper) interface. *Rev. Sci. Instrum.* **2006**, *77*, 116108.
(34) Heres, M.; Cosby, T.; Mapesa, E. U.; Sangoro, J. Probing nanoscale ion dynamics in ultrathin films of polymerized ionic liquids by broadband dielectric spectroscopy. *ACS Macro Lett.* **2016**, *5*, 1065−1069.
(35) Havriliak, S.; Negami, S. A Complex plane representation of dielectric and mechanical relaxation processes in some polymers. *Polymer* **1967**, *8*, 161−210.
(36) Tress, M.; Mapesa, E. U.; Kossack, W.; Kipnusu, W. K.; Reiche, M.; Kremer, F. Molecular dynamics in condensed (semi-) isolated polymer chains. In *Advances in Dielectrics*; Kremer, F., Ed.; Springer: Heidelberg, 2014; pp 61−94.
(37) Cheng, S.; Sokolov, A. P. Correlation between the temperature evolution of the interfacial region and the growing dynamic cooperativity length scale. *J. Chem. Phys.* **2020**, *152*, 094904.
(38) Pandey, Y. N.; Doxastakis, M. Detailed atomistic Monte Carlo simulations of a polymer melt on a solid surface and around a nanoparticle. *J. Chem. Phys.* **2012**, *136*, 094901.
(39) Pandey, Y. N.; Papakonstantopoulos, G. J.; Doxastakis, M. Polymer/nanoparticle interactions: bridging the gap. *Macromolecules* **2013**, *46*, 5097−5106.
(40) Rissanou, A. N.; Papananou, H.; Petrakis, V. S.; Doxastakis, M.; Andrikopoulos, K. S.; Voyiatzis, G. A.; Chrissopoulou, K.; Harmandaris, V.; Anastasiadis, S. H. Structural and conformational properties of poly(ethylene oxide)/silica nanocomposites: effect of confinement. *Macromolecules* **2017**, *50*, 6273−6284.
(41) Nguyen, H. K.; Labardi, M.; Capaccioli, S.; Lucchesi, M.; Rolla, P.; Prevosto, D. Interfacial and annealing effects on primary α-relaxation of ultrathin polymer films investigated at nanoscale. *Macromolecules* **2012**, *45*, 2138−2144.
(42) Forrest, J. A.; Dalnoki-Veress, K. When does a glass transition temperature not signify a glass transition? *ACS Macro Lett.* **2014**, *3*, 310−314.
(43) Boucher, V. M.; Cangialosi, D.; Yin, H.; Schönhals, A.; Alegría, A.; Colmenero, J. Tg depression and invariant segmental dynamics in polystyrene thin films. *Soft Matter* **2012**, *8*, 5119−5122.
(44) Solar, M.; Paul, W. Dielectric α-relaxation of 1,4-Polybutadiene confined between graphite walls: molecular dynamics investigations through numerical simulations of polymer molecules relaxation. *Eur. Phys. J. E: Soft Matter Biol. Phys.* **2015**, *38*, 123.
(45) Doxastakis, M.; Theodorou, D. N.; Fytas, G.; Kremer, F.; Faller, R.; Müller-Plathe, F.; Hadjichristidis, N. Chain and local dynamics of polyisoprene as probed by experiments and computer simulations. *J. Chem. Phys.* **2003**, *119*, 6883−6894.
(46) Provencher, S. W. CONTIN: A general purpose constrained regularization program for inverting noisy linear algebraic and integral equations. *Comput. Phys. Commun.* **1982**, *27*, 229−242.
(47) Provencher, S. W. Inverse problems in polymer characterization: direct analysis of polydispersity with photon correlation spectroscopy. *Makromol. Chem.* **1979**, *180*, 201−209.
(48) Andrews, R. N.; Narayanan, S.; Zhang, F.; Kuzmenko, I.; Ilavsky, J. CONTIN XPCS: Software for inverse transform analysis of X-ray photon correlation spectroscopy dynamics. *J. Appl. Crystallogr.* **2018**, *51*, 205−209.
(49) Williams, G.; Watts, D. C. Non-Symmetrical dielectric relaxation behaviour arising from a simple empirical decay function. *Trans. Faraday Soc.* **1970**, *66*, 80−85.
(50) Tyagi, M.; Alegria, A.; Colmenero, J. Heterogeneous dynamics of poly(vinyl acetate) far above Tg: a combined study by dielectric spectroscopy and quasielastic neutron scattering. *J. Chem. Phys.* **2005**, *122*, 244909.
(51) Tammann, V. G.; Hesse, W. Die Abhängigkeit der Viscosität von der Temperatur bie unterkühlten Flüssigkeiten. *Z. Anorg. Allg. Chem.* **1926**, *156* (1), 245−257.
(52) Vogel, H. The law of the relationship between viscosity of liquids and the temperature. *Phys. Z.* **1921**, *22*, 645−646.
(53) Fulcher, G. S. Analysis of recent measurements of the viscosity of glasses - Reprint. *J. Am. Ceram. Soc.* **1992**, *75*, 1043−1059.
(54) Vogel, M. Rotational and conformational dynamics of a model polymer melt at solid interfaces. *Macromolecules* **2009**, *42*, 9498−9505.
(55) Arndt, M.; Stannarius, R.; Gorbatschow, W.; Kremer, F. Dielectric investigations of the dynamic glass transition in nanopores.

https://dx.doi.org/10.1021/acs.jpclett.0c03211
J. Phys. Chem. Lett. 2021, 12, 117−125

Phys. Rev. E: Stat. Phys., Plasmas, Fluids, Relat. Interdiscip. Top. **1996**, *54*, 5377−5390.
(56) Stannarius, R.; Kremer, F.; Arndt, M. Dynamic exchange effects in broadband dielectric spectroscopy. *Phys. Rev. Lett.* **1995**, *75*, 4698−4701.
(57) Paeng, K.; Ediger, M. D. Molecular motion in free-standing thin films of poly(methyl methacrylate), poly(4-tert-butylstyrene), poly(α-methylstyrene), and poly(2-vinylpyridine). *Macromolecules* **2011**, *44*, 7034−7042.
(58) Paeng, K.; Lee, H. N.; Swallen, S. F.; Ediger, M. D. Temperature-ramping measurement of dye reorientation to probe molecular motion in polymer glasses. *J. Chem. Phys.* **2011**, *134*, 024901.
(59) Paeng, K.; Swallen, S. F.; Ediger, M. D. Direct measurement of molecular motion in freestanding polystyrene thin films. *J. Am. Chem. Soc.* **2011**, *133*, 8444−8447.

https://dx.doi.org/10.1021/acs.jpclett.0c03211
J. Phys. Chem. Lett. 2021, 12, 117−125

SUPPORTING INFORMATION

Interfacial Dynamics in Supported Ultrathin Polymer Films – From the Solid to the Free Interface

Emmanuel Urandu Mapesa[†], Nobahar Shahidi[†], Friedrich Kremer[‡], Manolis Doxastakis[†*] & Joshua Sangoro[†*]

†Department of Chemical and Biomolecular Engineering, University of Tennessee Knoxville, 1512 Middle Dr., Knoxville, TN-37996, USA.
‡Department of Molecular Physics, Peter Debye Institute of Soft Matter Physics, University of Leipzig, Linnéstr. 5, 04103 Leipzig, Germany.

.

1. Experimental and Simulation Details

1.1 Experimental. Poly(vinyl acetate) (PVAc) samples with molecular weight, M_w, equal to 110 kg/mol (PDI = 2, Polymer Source Inc.) and 157 kg/mol (PDI = 2.3, Scientific Polymer Products) were used as received without any further purification. Chloroform (purity ≥99.8%, Sigma Aldrich) was used as solvent to dissolve the polymers. The procedure used for film preparation is published elsewhere.[2] Bearing in mind that the boiling point of chloroform is 335 K and that PVAc degrades in vacuum at temperatures above 500 K,[3] the films were annealed at 400 K for 24 h in an oil-free vacuum (10^{-6} mbar) in order to relax them and remove solvent. All films reported in this work had a post-BDS measurement root mean square roughness less than 2 nm on a scan area of 20 μm^2. For dielectric investigations, the sample capacitors containing thin films were assembled using a nanostructured electrode arrangement (see schematic in Inset, Fig. 1b) where a regular array of highly insulating silica nano-pillars (base area 5μm x 5μm, height ~70nm, and an inter-pillar separation of 45μm) serves as separation to ensure electrical isolation. Ultraflat (rms roughness of 0.6 nm on a micrometric scale) and highly conductive (resistivity < 5 mΩ cm) silicon wafers are used as electrodes. For detailed information on the use of this capacitor configuration and cleaning procedures, the reader is referred previous publications by some of the current authors[2, 4-7]. Bulk samples were measured using 20 mm stainless steel electrodes in a parallel-plate configuration with 100 μm teflon spacers to maintain sample thickness. All dielectric measurements were carried out on a high resolution Novocontrol Alpha Analyzer (frequency range 10^{-1} – 10^{7} Hz) and the temperature control regulated by a QUATRO system (Novocontrol) using a jet of dry nitrogen, thereby ensuring relative and absolute errors better than 0.1 and 2 K, respectively.

1.2 MD Simulations. Molecular dynamics (MD) simulations were performed with the GROMACS 2018.3 package.[8-9]Atactic poly(vinyl acetate) was modeled with the atomistic OPLS-AA force-field for hydrocarbons.[10-11] An atomistic model of amorphous silica was employed to simulate the oxidized layer in contact with the films in BDS experiments. The nonbond parameters for silica were taken from Berendsen *et al*.[8] and Ndoro *et al*.[12]; the bonded parameters and initial structure were adopted from Pandey and Doxastakis[13], and hydrogens added to the structure. The simulations were performed with a 2 fs time step with semi-isotropic pressure coupling using the Berendsen barostat[14] and stochastic velocity rescaling thermostat[15] with a time step of 1.0 ps and 0.1 ps, respectively. The box depth in the *z* dimension was kept constant to include vacuum on top of PVAc. Non-bonded interactions were switched to zero at 1.3 nm and a reaction field was employed for the coulombic interactions with the relative dielectric constant of $\varepsilon_{rf} = 3.8$ (taken from the average experimental dielectric constant of silica and poly(vinyl acetate) at room temperature[12, 16]). The bulk with N = 10 monomers has a density of 1073 kg/m^3 at 400 K which is in agreement with experimental value of 1107 kg/m^3.[17] PVAC films each contained 614 chains with 10 repeat units (Mw = 0.86 kg/mol) and were simulated at temperatures of 560, 530, 500, 480, 460, 430 and 400 K at 1 bar. The films were each equilibrated for 200, 250, 300, 450, 450 ns and 1.5 μs resulting in thin films with thickness ranging from 13.4 to 17 nm, as the temperature decreases.

2. Typical dielectric spectra of bulk and ultrathin PVAc films

The normalized dielectric data for the series of 157 kg/mol polymer films is given below (Fig. S1) to highlight the broadening of the distributions of relaxation times with decreasing film thickness. A comparison of the experimental and simulations data is also given in Figure S3.

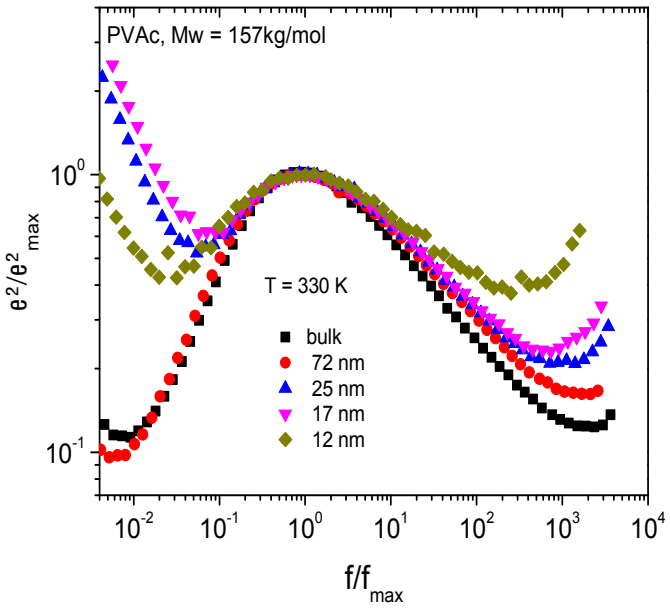

FIGURE S1. **Data measured at 330 K showing the dielectric loss data as a function of frequency normalized with respect to the maximum loss for PVAc (Mw = 157 kg/mol) samples ranging in size from bulk dimensions (thickness, ~100 μm) to thin films, with thicknesses as indicated.**

2. Reorientation of Backbone Torsion

The backbone dihedral autocorrelation is compared with the monomer dipole autocorrelation in Figure S2. Although the main component of the dipole is located in the sidechain, the re-orientation of the backbone plays an important part in the segmental relaxation. The two measures of segmental dynamics follow a similar trend. The dihedral autocorrelation probes larger segments and is slower at longer times.

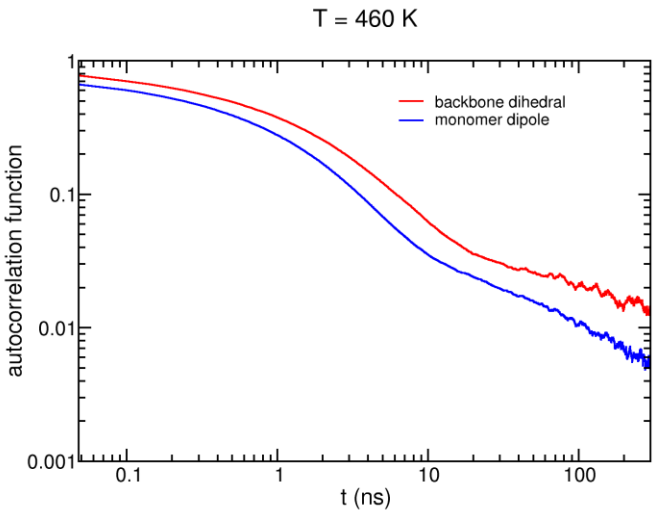

FIGURE S2 **The monomer dipole and backbone dihedral autocorrelation functions for the thin film at 460 K.**

3. Comparison: Raw experimental and simulations data

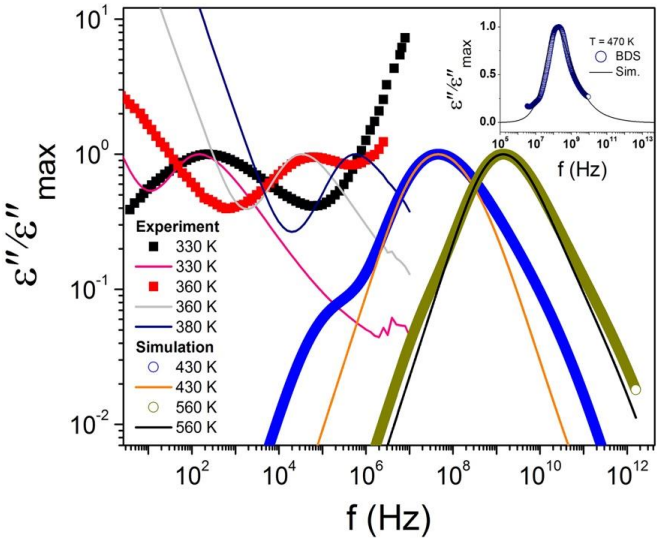

FIGURE S3. **Dielectric loss as a function of frequency as determined experimentally and by simulation at different temperatures. Square and circle symbols represent data for thin films while the lines are bulk data. Inset: Simulation data for the bulk system compared to BDS data from Tyagi *et al.*[1] at 470 K.**

4. Analysis of dielectric data of the ultrathin polymer films

The spectra for the thin films have more features arising from contributions of the thermally oxidized silica layer on the Si wafers, the silica nano-spacers, the polymeric film, the gap between the film layer and the spacers, and the wafers, with respective complex capacitances C_o^*, C_{sp}^*, C_{film}^*, C_{gap}^*, and C_w^*. The total complex capacitance is therefore calculated by considering the serial arrangement of the constituent capacitors as

$$\left(C_{total}^*\right)^{-1} = 2\left(C_w^*\right)^{-1} + \left(C_{sp,eff}^*\right)^{-1} + \left(C_{gap}^*\right)^{-1} + \left(C_{film}^*\right)^{-1} + \left(C_o^*\right)^{-1} \quad \text{…[Eq. S1]}$$

where $C_{sp,eff}^*$ is the effective complex capacitance of the spacers and the free space between them, the two of them being in parallel arrangement to each other with respect to the applied field.

The total complex dielectric function that describes the measured data is

$$\frac{D}{\varepsilon_{total}^*} = \frac{2d_w}{\varepsilon_w^*} + \frac{d_{sp}}{\left(\rho_{sp}\varepsilon_{sp}^* + 1 - \rho_{sp}\right)} + \frac{d_{gap}}{\varepsilon_{gap}^*} + \frac{d_{film}}{\varepsilon_{film}^*} + \frac{d_o}{\varepsilon_o^*} \quad \text{…[Eq. S2]}$$

where D is the distance between the two electrodes, ρ_{sp} is density of coverage of the nano-spacers, d_x is a thickness with the respective subscripts having meanings already introduced. The thicknesses of the wafers, the nano-spacers, the oxide on the wafers and that of the thin films are known, in addition to setting $\varepsilon_{gap}^* = 1$, thus reducing the fit parameters. ε_{film}^* is substituted with three Havriliak-Negami functions. Suffice it to mention that because it is experimentally not possible to determine the height of the gap, d_{gap}, it is treated as a fit parameter in the analysis, which effectively means that we cannot accurately determine the relaxation strength of the polymeric layer. Several other modifications of Eq. S2 to account for more complicated experimental possibilities of this geometry have been considered – as comprehensively detailed in

Tress *et al.*[18] – and are found to deliver negligible changes to the shape parameters and position of the α-peak obtained from the HN function of the polymeric layer.

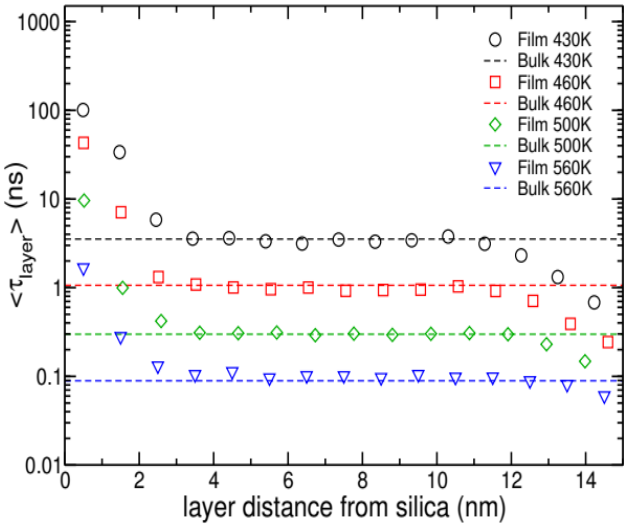

FIGURE S4. **Average relaxation time for monomers at different film layers parallel to silica. The dashed lines represent the bulk relaxation time at each temperature.**

We turn our focus now to the effect of the polymer/silica and the polymer/free vacuum interfaces on dynamics by systematically probing segmental motion in different layers throughout the film. The layers are defined based on the center of mass distance of the monomers from the silica surface and are each about 1 nm thick. The monomer dipole autocorrelation function (φ_{layer}(t)) is calculated for monomers that are in the layer at time t from the total monomer dipole moment to improve the statistics. The average relaxation time for each layer ($< \tau_{layer} >$) is calculated as $< \tau_{layer} > = \int_0^\infty \varphi_{layer}(t)dt$ and presented in Figure S4 as a function of layer distance from the silica interface at different temperatures. Based on the profile of the relaxation times throughout the film, we define three main layers. Similar to the density profile (Fig. S8), the middle layer away from the two interfaces has bulk-like dynamics. The bottom layer (near the substrate) has much slower dynamics (more than 10 times slower than bulk); the thickness of this bottom layer is ~4 nm and does not have a strong correlation with temperature. However, the contribution of the bottom layer to overall film dynamics increases with decreasing temperature since the fraction of monomers near the substrate increases with density. Finally, segmental relaxation is faster in the top layer (close to the vacuum interface), and its thickness and mole fraction increase at low temperatures. The relaxation time of the free segments near the vacuum approaches the bulk value at high temperatures hence the decrease in top layer thickness as defined here. Notably, the thickness of the layers as defined by dynamics is different from that determined from the density profile.

5. Estimation of segmental dynamics from simulations

Segmental relaxation can be estimated as a superposition of Debye relaxations. The autocorrelation function of bulk PVAc can be fitted with a Kohlrausch-Williams-Watts (KWW) function[19] and the film can be fitted as a sum of two stretched exponentials that represent the separate processes:

$$\varphi_{K,film} = \alpha_m \exp\left(-\left(\frac{t}{\tau_m}\right)^{\beta_m}\right) + \alpha_s \exp\left(-\left(\frac{t}{\tau_s}\right)^{\beta_s}\right) \ldots \text{[Eq. S3]}$$

where τ is the KWW relaxation time and β describes the heterogeneity of the distribution of relaxation times. The α parameter in equation represents the weight of each term in the autocorrelation function. Using the KWW fits we extracted the average characteristic time ($< \tau >$) for each process:

$$< \tau_i > = \frac{\alpha_i}{\beta_i} \Gamma\left(\frac{1}{\beta i}\right) \tau_i \ldots \text{[Eq. S4]}$$

where subscript i represents the main bulk-like process (m) or the slow process (s).

The sum of α_m and α_s in Eq. S3 is less than 1 since we do not fit the initial relaxation caused by the fast-vibrational motions. The weight of the bulk-like relaxation, α_m is about 0.8 while the slow process has a small contribution ($\alpha_s \approx 0.15$). The relaxation time of the first process (τ_m) has a similar value to bulk. As expected τ increases at lower temperatures for both processes but follows different temperature trends with τ_s approaching τ_m as the temperatures increase. The β_s parameter is generally lower than β_m as the dynamics become more heterogeneous close to the substrate. The bulk-like relaxation also become less heterogeneous at higher temperatures.

The complex dielectric permittivity, ε^*, in the frequency domain is the Fourier transform of the derivative of the dipole autocorrelation function

$$\frac{\varepsilon^* - \varepsilon_\infty}{\Delta\varepsilon} = 1 - i\omega \int_0^\infty \frac{d\varphi(t)}{dt} \exp(-i\omega t)\, dt \ldots \text{[Eq. S5]}$$

The calculated permittivity is normalized by the difference in permittivity at the infinite (ε_∞) and zero (ε_0) limit of frequency. The equivalent loss (ε") profile is calculated as given in Eq. S6 using the distribution of relaxation times to directly compare the simulation results with BDS data.

$$\frac{\varepsilon''}{\varepsilon_\infty - \varepsilon_0} = \sum_\tau \psi(\tau) \frac{\omega\tau}{1+(\omega\tau)^2} \ldots \text{[Eq. S6]}$$

The measured and computed loss data for films is displayed at different temperatures in Figure S3. The simulation results show excellent agreement with BDS data for bulk at 470 K (see inset, Fig. S3). The simulation results in this figure underscore the fact that the slow relaxation, α_{slow}, becomes more prominent with decreasing temperature. Also, while α_{fast} does not show up in the simulation data as a separate relaxation, there's evidence of broadening of the spectra on the high-frequency side, indicating the presence of new faster modes.

6. Molecular weight dependence of segmental dynamics

The segmental dynamics of PVAc oligomers depends on molecular weight until the density plateaus (at about 11000) .[20] Figure S5 displays the total monomer dipole autocorrelation for the film and bulk at 560 K at two different chain lengths N=10 monomers (Mw = 860 g/mol, ρ = 0.945 g/cm^3) and N = 30 (Mw = 2582 g/mol, ρ = 0.975 g/cm^3). Both systems show a similar trend in dynamics with a bulk-like relaxation and a second slow at higher times. The dynamics in the N=30 system is slower due to the higher density and the difference between two modes in film is more apparent. The average film relaxation time that is about 5 times larger than bulk for N = 30 and 1.6 time larger for N = 10.

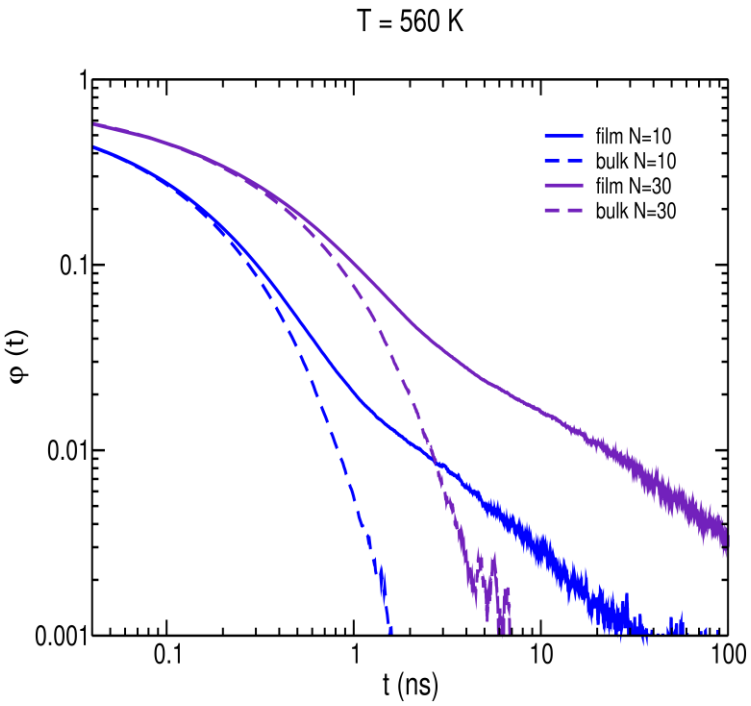

FIGURE S5. **Segmental dynamics of film and bulk at two different chain lengths, N=10 monomers and N=30 monomers at 560 K.**

Figure S6 compares the single-chain dipole autocorrelation with monomer dipole autocorrelation for chains with N = 10 monomers at 560 K. Probing the monomer dipole autocorrelation improves the statistics and enables a more detailed analysis of dynamics throughout the film thickness. The chain segmental relaxation is qualitatively similar to the monomer autocorrelation with an even slower decay for the adsorbed segments when cross-correlations between monomers are accounted for. The average relaxation time for chain dipole autocreation in film is 7.5 larger than bulk.

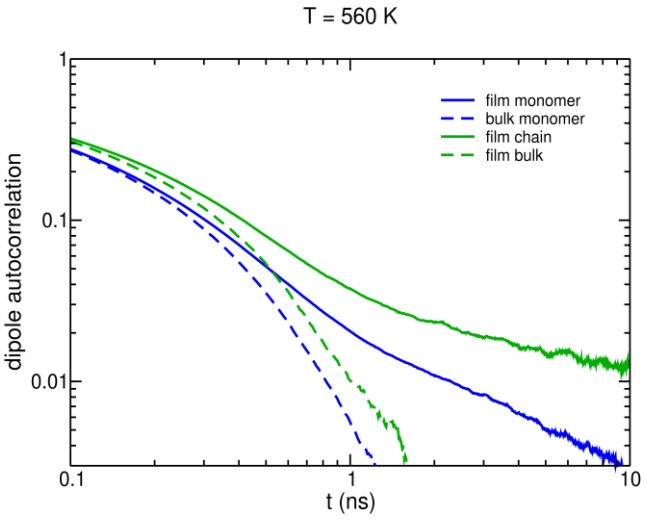

FIGURE S6. **Monomer dipole autocorrelation and chain dipole autocorrelation for film and bulk for chains with N = 10 monomers at 560 K.**

7. Estimating the size of layers with modified mobility

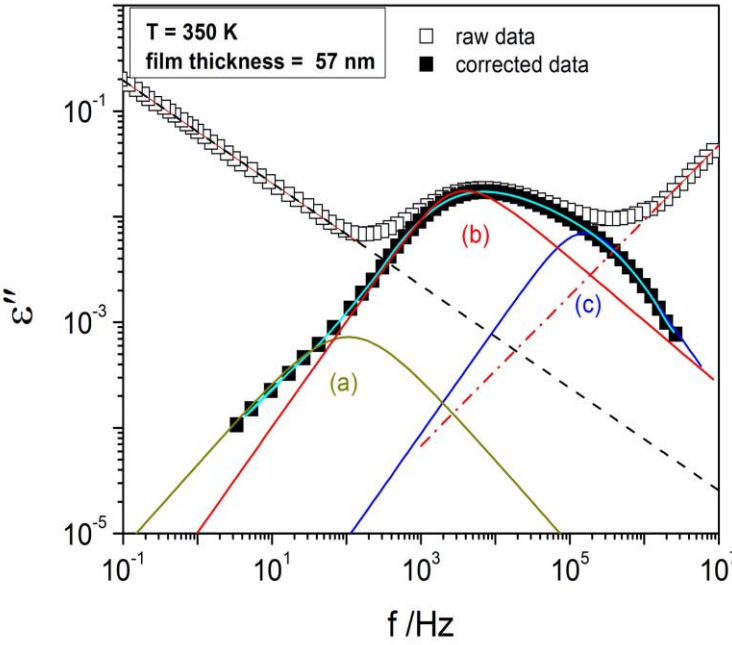

FIGURE S7. **Dielectric loss plotted as a function of frequency for the as-measured data (open squares), and corrected data, i.e., after subtraction of the low- and high-frequency flanks (closed squares). (a), (b) and (c) are HN functions needed to fit the corrected data.**

The conductivity contribution (low frequency flank) and that due to limited conductivity of the silicon electrodes (on the high-frequency side) were first subtracted from the measured dielectric loss. The former contribution is estimated by a linear function (dashed line) while the latter is described by a Debye-like function (dash-dotted line – which is the low-frequency wing of the said Debye-like function). Three Havriliak Negami (HN) functions are required to fit the corrected spectrum. These calculations were carried out on the data measured in a cooling run. Given that the overall film thickness is known from AFM measurements, the layers corresponding to processes (a), (b) and (c) in Figure S7 were assumed to be stacked together and estimated from the corresponding value of Δε. For instance, for a film with overall thickness of D nm, the size of the layer, d_a, with slowed mobility is calculated as $d_a = D\,\Delta\varepsilon_a/(\Delta\varepsilon_a + \Delta\varepsilon_b + \Delta\varepsilon_c)$, where the subscripts derive from the representation in Figure S7. To estimate the uncertainty inherent in the obtained values of the layer sizes, this procedure was repeated for (some select) data measured in a heating run. The deviation from the arithmetic mean of the two values of layer thickness at a given temperature is taken as a representative measure of the error in our calculations. The error bars in Figure 5 (main paper) represent this random uncertainty.

In Figure S8, normalized dielectric strength for the three layers is plotted against inverse temperature. The values are normalized with respect to that found at the lowest accessed temperature (330 K). Since Δε is used to estimate layer thickness, the consistent trend seen in Figure S7 underscores the veracity of this approach.

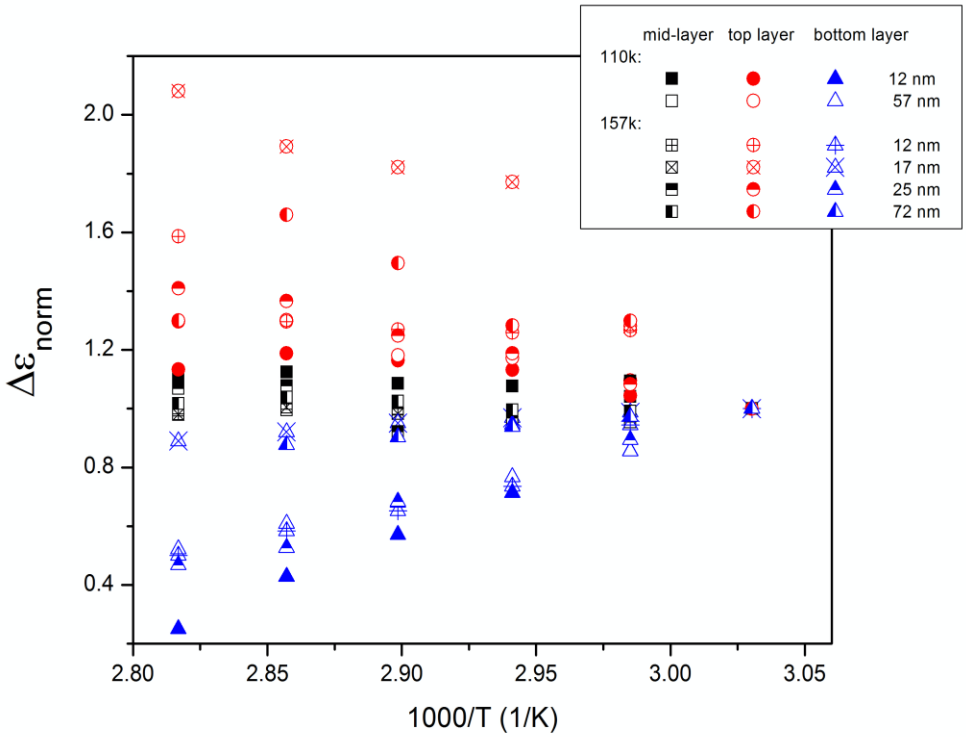

FIGURE S8. **Dielectric relaxation strength for the three different layers (normalized with respect to the value at 330 K) presented as a function of inverse temperature.**

8. Layer thickness from density (computation)

Figure S9 shows the density profile for the PVAc film and bulk from MD simulations at 460 and 560 K. The density is displayed as a function of distance from the substrate. Each bin displays the density for a layer normal to the *z*-direction with ~0.1 nm thickness. Accumulation of segments near the attractive substrate results in a peak at the adsorbed layer[21-25] at ~0.7 nm. The effect of the substrate on density is short-ranged and after ~1.6 nm the density decays to a plateau that matches the bulk density. The drop in density from the bulk value at the top of the film marks the vacuum interface.

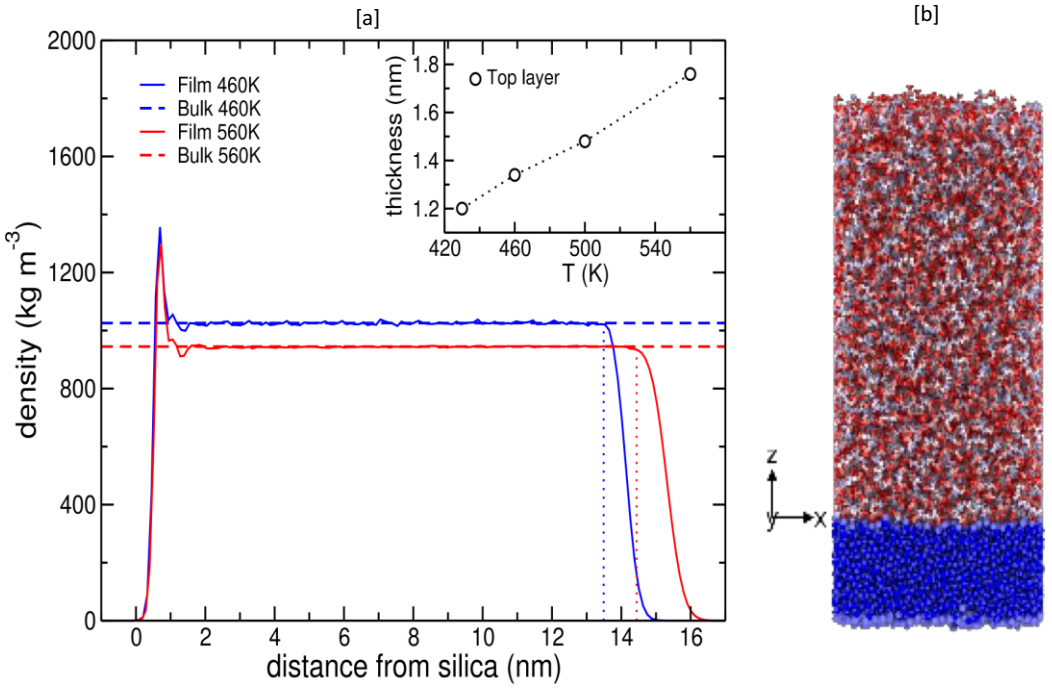

FIGURE S9. **(a) Density profile of the film in the z-direction at 460 K (blue) and 560 K (red). The dashed lines represent the bulk density. The dotted lines separate the vacuum interface from hyperbolic tangent function fits. (b) shows a typical configuration of PVAc film on silica as employed in the simulation. Inset: estimate of the size of the top layer from density calculations.**

The density decays to zero at the vacuum interface at the top of the film. This drop was fitted with the hyperbolic tangent function to determine the position of the interface (separated with dotted lines in Fig. S9).

$$\rho(z) = \frac{\rho_{bulk}}{2}\left(1 - \tanh\left(\frac{2(z-z_e)}{\delta}\right)\right) \ldots \text{[Eq. S7]}$$

The width of the vacuum interface (equal to 2δ from the above equation) gradually expands with temperature as displayed in the inset of Fig. S9). The thickness of the absorbed layer as determined by the position of the first peak shows little change with temperature.

8. Layer thickness from dielectric relaxation strength (experimental)

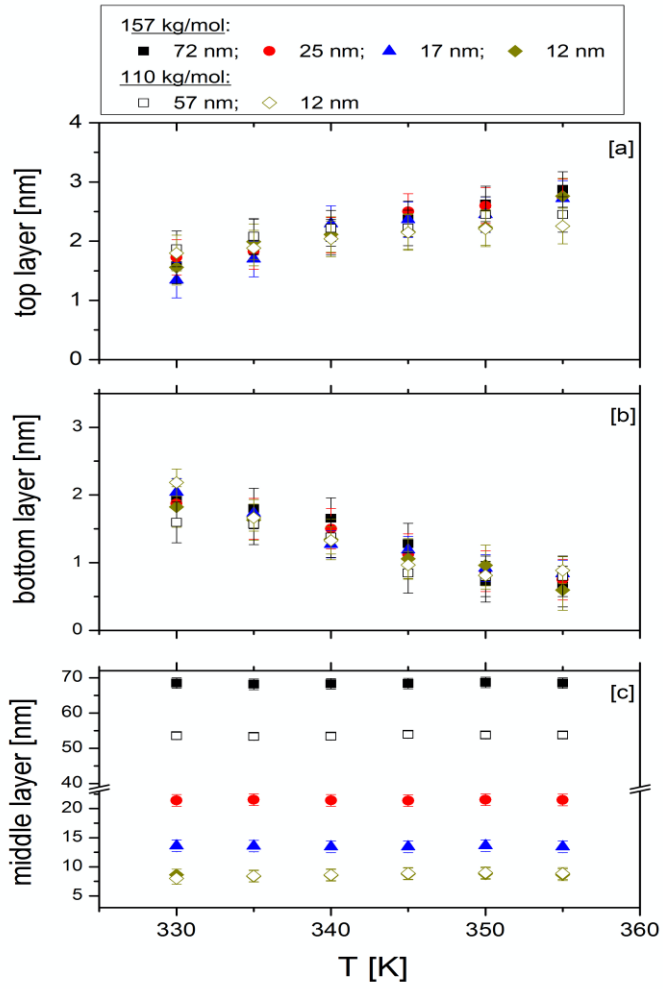

FIGURE S10. **The size, in nanometers, of layers whose mobility is (a) increased (top layer), (b) slowed-downed (bottom layer) and (c) bulk-like (middle layer) expressed as functions of temperature for films prepared from two different molecular weights of PVAc, as indicated.**

References

(1) Tyagi, M.; Alegria, A.; Colmenero, J. Heterogeneous Dynamics of Poly(vinyl acetate) Far Above Tg: A combined study by dielectric spectroscopy and quasielastic neutron scattering. *J. Chem. Phys.* **2005,** *122* (24), 244909.

(2) Mapesa, E. U.; Tress, M.; Schulz, G.; Huth, H.; Schick, C.; Reiche, M.; Kremer, F. Segmental and chain dynamics in nanometric layers of poly(cis-1,4-isoprene) as studied by broadband dielectric spectroscopy and temperature-modulated calorimetry. *Soft Matter* **2013,** *9* (44), 10592-10598.

(3) Blazevska-Gilev, J.; Spaseska, D. Thermal degradation of PVAc. *J. Univ. Chem. Technol. and Metal.* **2005,** *40* (4), 287-290.

(4) Serghei, A.; Kremer, F. Broadband dielectric studies on the interfacial dynamics enabled by use of nanostructured electrodes. *Rev. Sci. Instr.* **2008,** *79* (2), 026101.

(5) Tress, M.; Erber, M.; Mapesa, E. U.; Huth, H.; Müller, J.; Serghei, A.; Schick, C.; Eichhorn, K.-J.; Voit, B.; Kremer, F. Glassy dynamics and glass transition in nanometric thin layers of polystyrene. *Macromolecules* **2010,** *43* (23), 9937-9944.

(6) Mapesa, E. U.; Erber, M.; Tress, M.; Eichhorn, K. J.; Serghei, A.; Voit, B.; Kremer, F. Glassy dynamics in nanometer thin layers of polystyrene. *Eur. Phys. J. Spec. Top.* **2010,** *189* (1), 173-180.
(7) Serghei, A.; Kremer, F. Broadband dielectric spectroscopy on ultrathin organic layers having one free (upper) interface. *Rev. Sci. Instrum.* **2006,** *77* (11), 116108.
(8) Berendsen, H. J. C.; Spoel, D. v. d.; Drunen, R. v. GROMACS: A message-passing parallel molecular dynamics implementation. *Comput. Phys. Commun.* **1995,** *91* (1), 43-56.
(9) Abraham, M. J.; Murtola, T.; Schulz, R.; Páll, S.; Smith, J. C.; Hess, B.; Lindahl, E. GROMACS: High performance molecular simulations through multi-level parallelism from laptops to supercomputers. *SoftwareX* **2015,** *1-2*, 19-25.
(10) Lopes, P. E. M.; Murashov, V.; Tazi, M.; Demchuk, E.; MacKerell, A. D. Development of an empirical force field for silica. Application to the quartz−water interface. *J. Phys. Chem. B* **2006,** *110* (6), 2782-2792.
(11) Price, M. L. P.; Ostrovsky, D.; Jorgensen, W. L. Gas-phase and liquid-state properties of esters, nitriles, and nitro compounds with the OPLS-AA force field. *J. Comput. Chem.* **2001,** *22* (13), 1340-1352.
(12) Ndoro, T. V. M.; Voyiatzis, E.; Ghanbari, A.; Theodorou, D. N.; Böhm, M. C.; Müller-Plathe, F. Interface of grafted and ungrafted silica nanoparticles with a polystyrene matrix: atomistic molecular dynamics simulations. *Macromolecules* **2011,** *44* (7), 2316-2327.
(13) Pandey, Y. N.; Doxastakis, M. Detailed atomistic Monte Carlo simulations of a polymer melt on a solid surface and around a nanoparticle. *J. Chem. Phys.* **2012,** *136* (9), 094901.
(14) Berendsen, H. J. C.; Postma, J. P. M.; van Gunsteren, W. F.; DiNola, A.; Haak, J. R. Molecular dynamics with coupling to an external bath. *J. Chem. Phys.* **1984,** *81* (8), 3684-3690.
(15) Provencher, S. W. A Constrained regularization method for inverting data represented by linear algebraic or integral equations. *Comput. Phys. Commun.* **1982,** *27*, 213-227.
(16) Lide, D. R.; Milne, G. W. A. *CRC Handbook of Data on Organic Compounds*. CRC Press: 1993.
(17) Mark, J. E. *Physical Properties of Polymers Handbook*. Springer: Berlin, 2007; Vol. 1076.
(18) Tress, M.; Mapesa, E. U.; Kossack, W.; Kipnusu, W. K.; Reiche, M.; Kremer, F. Molecular dynamics in condensed (semi-) isolated polymer chains. In *Advances in Dielectrics*, Kremer, F., Ed. Springer: Heidelberg, 2014; pp 61-94.
(19) Williams, G.; Watts, D. C. Non-symmetrical dielectric relaxation behaviour arising from a simple empirical decay function. *J. Chem. Soc. Faraday Trans.* **1970,** *66*, 80-85.
(20) Negami, S.; Ruch, R. J.; Myers, R. R. The dielectric behavior of poly(vinyl acetate) as a function of molecular weight. *J. Colloid Interface Sci.* **1982,** *90*, 117-226.
(21) Rissanou, A. N.; Harmandaris, V. Dynamics of various polymer-graphene interfacial systems through atomistic molecular dynamics simulations. *Soft Matter* **2014,** *10* (16), 2876-88.
(22) Mortazavian, H.; Fennell, C. J.; Blum, F. D. Structure of the interfacial region in adsorbed poly(vinyl acetate) on silica. *Macromolecules* **2015,** *49* (1), 298-307.
(23) Mathieu, S.; Binder, K.; Paul, W. Dielectric relaxation of a polybutadiene melt at a crystalline graphite surface: atomistic molecular dynamics simulations. In *Dynamics in Geometrical Confinement*, Kremer, F., Ed. Springer International Publishing: Berlin, 2014; pp 1-15.
(24) Yelash, L.; Virnau, P.; Binder, K.; Paul, W. Slow process in confined polymer melts: layer exchange dynamics at a polymer solid interface. *Phys. Rev. E Stat. Nonlin. Soft Matter Phys* **2010,** *82* (5 Pt 1), 050801.
(25) Yelash, L.; Virnau, P.; Binder, K.; Paul, W. Three-step decay of time correlations at polymer-solid interfaces. *Europhys. Lett.* **2012,** *98* (2), 28006.